Automatica 45 (2009) 1649–1658

Contents lists available at ScienceDirect

Automatica

journal homepage: www.elsevier.com/locate/automatica

Design, analysis and experimental validation of a robust nonlinear path following controller for marine surface vessels☆

Zhen Li *, Jing Sun, Soryeok Oh

Department of Naval Architecture and Marine Engineering, University of Michigan, Ann Arbor, MI, 48109, USA

ARTICLE INFO

Article history:
Received 27 March 2008
Received in revised form
5 January 2009
Accepted 11 March 2009
Available online 11 April 2009

Keywords:
Ship control
Path following
Nonlinear control
Backstepping
Marine surface vessels

ABSTRACT

The problem of path following for marine surface vessels using the rudder angle is addressed in this paper. A four-degree-of-freedom nonlinear surface vessel model, together with the Serret–Frenet equations, is introduced to describe the ship dynamics and path following error dynamics. While similar models have been used and reported in the literature for path following control algorithm development, the novelty of the approach presented in this work lies in the following aspects. (a) The back-stepping nonlinear controller design is based on feedback dominance, instead of feedback linearization and nonlinearity cancelation; (b) additional design parameters are employed in the Lyapunov function that lead to simplification of the controller in the design procedure and normalization of different variables in the Lyapunov function to improve the controller performance; (c) relying on feedback dominance and the introduction of the additional parameters in the Lyapunov function, the resulting controller is almost linear, with very benign nonlinearities allowing for analysis and evaluation; and (d) the performance of the nonlinear controller, in terms of path following, is analyzed for robustness in the presence of model uncertainties. The simulation results are presented to verify and illustrate the analytic development and the effectiveness of the resulting control against rudder saturation and rate limits, and delays in the control execution, as well as measurement noises. Furthermore, the control design is validated by experimental results conducted in a tank using a model ship.

1. Introduction

Controlling of marine surface vessels to follow a prescribed path or track a given trajectory has been a representative control problem for marine applications and it has attracted considerable attention from the control community. One challenge for path following of a surface marine vessel stems from the fact that the system is often underactuated. Conventional ships are usually equipped with one or two main propellers for forward speed control, and rudders for course keeping of the ship. For ship maneuvering problems, such as path following and trajectory tracking, where we seek control for all three degrees of freedom (surge, sway, and yaw), the two controls cannot influence all three variables independently, thereby leading to underactuated control problems. In conventional way-point guidance systems, the output space is reduced such that the number of outputs equals the number of control inputs, and a fully actuated control problem can be formulated (Fossen, Breivik, & Skjetne, 2003). In most cases, the three-degree-of-freedom (3-DoF) problem is reduced to controlling the yaw angle and surge velocity. Recent development (Do & Pan, 2003, 2006; Do, Jiang, & Pan, 2002, 2004; Fossen et al., 2003; Jiang, 2002; Lefeber, Pettersen, & Nijmeijer, 2003; Pettersen & Lefeber, 2001) in nonlinear control and control of underactuated systems, however, has offered new tools and promising solutions to deal with all three degrees of freedom using two independent controls.

Another challenge in the path following of marine surface vessels is the inherent nonlinearity, from either the ship dynamics or path following kinematics. Many different nonlinear design methodologies have been attempted. For example, Lyapunov's direct method is used in Breivik and Fossen (2004b) and Jiang (2002) while cascade control is employed in Lefeber et al. (2003) and Pettersen and Lefeber (2001). Most papers published on this topic adopt back-stepping as the design methodology (Do & Pan, 2003; Do et al., 2002, 2004; Encarnacao & Pascoal, 2001; Fossen et al., 2003; Lapierre, Soetanto, & Pascoal, 2003; Pettersen & Nijmeijer, 1998; Skjetne & Fossen, 2001; Skjetne, Fossen, & Kokotovic, 2004). Instead of using linear

☆ This work is supported by the Office of Naval Research under grants N00014-05-1-0537 and N00014-06-1-0879. The material in this paper was partially presented at IFAC Conference on Control Applications in Marine Systems, Bol, Croatia, 2007. This paper was recommended for publication in revised form by Associate Editor Uwe R. Zimmer under the direction of Editor Toshiharu Sugie.

* Corresponding author. Tel.: +1 734 615 8061, +1 734 330 8418; fax: +1 734 936 8820.

E-mail addresses: lizhen@umich.edu (Z. Li), jingsun@umich.edu (J. Sun), srohum@umich.edu (S. Oh).

0005-1098/$ – see front matter © 2009 Elsevier Ltd. All rights reserved.
doi:10.1016/j.automatica.2009.03.010

approximations, they often explore the inherent nonlinearities to achieve better performance. However, since the controller attempts to cancel or compensate for high order nonlinearities, it yields a very complicated control law. Meanwhile, most of the control methodologies are explored with analytical and/or numerical investigations and no experimental efforts are reported, with the exception of Do and Pan (2006), Fossen et al. (2003), and Lefeber et al. (2003), where the Cybership (I and II) with an infrared camera system and a model ship with a Differential Global Positioning System (DGPS) are used for experimental validation, respectively.

Some path following algorithms for marine surface vessels, such as the LQR approach (Holzhuter, 1997) and PID-type controller (Kallstrom, 2000), have already achieved industrial applications. All of these industrial path following systems pay great attention to the robustness and easy implementation.

Motivated by these recent development in path following of marine surface vessels, this paper presents a novel back-stepping design for an integrated model of the surface vessel dynamics and 2-DoF path following kinematics. Our focus is on developing a controller that lends itself for easy tuning and implementation, which is one of the key considerations of industrial path following systems. A simplified 2-DoF linear model is adopted in the controller design and a 4-DoF model is used in simulations in order to study the interactions between the path following maneuvering control and seakeeping roll dynamics. The Serret–Frenet formulation from differential geometry represents the desired path as a two-dimensional smooth curve, which allows for convenient definition of continuous cross-track and heading error. The essence of the proposed back-stepping nonlinear controller design is to rely on feedback dominance, instead of feedback linearization and nonlinearity cancelation, in the control design procedure. Moreover, additional parameters are employed in the Lyapunov function to simplify the controller by manipulating these parameters to cancel the nonlinear terms without relying on feedback nonlinear cancelation. These parameters also provide the normalization effects for different variables in the Lyapunov function to improve the controller performance. This approach has led to a control law that is almost linear with very benign nonlinearities, thereby allowing for analytical study and evaluation. The path following capability of the proposed method and the robustness against model uncertainties are demonstrated through theoretical analysis, numerical simulations and also experimental validations.

A conference version of this paper was presented at the IFAC Conference on Control Applications in Marine Systems in 2007 (Li, Sun, & Oh, 2007). This paper expands the results in Li et al. (2007) by (a) including the detailed robustness analysis against unmodeled dynamics and (b) demonstrating the effectiveness of the proposed controller through experimental validations. The paper is organized as follows. In Section 2, the simplified 2-DoF linear model is presented along with the Serret–Frenet formulation to facilitate the path following control design. In Section 3, the path following control law based on the back-stepping method using feedback dominance is derived, and the control law is shown to have a simple expression. Section 4 is devoted to the robustness analysis of the resulting control system, where unmodeled dynamics are considered. The simulation results are presented in Section 5 and the experimental validation is summarized in Section 6, followed by the conclusions in Section 7.

2. Path following error dynamics and surface vessel model

In the open literature, the marine surface vessel path following problem has been addressed with two different approaches: one is to treat it as a tracking control problem (Do et al., 2002, 2004; Encarnacao & Pascoal, 2001; Jiang, 2002; Lefeber et al., 2003; Pettersen & Nijmeijer, 1998), and the other is to simplify the tracking control problem into a regulation control problem by adopting proper path following error dynamics (Breivik & Fossen, 2004a,b, 2005; Lapierre et al., 2003; Pettersen & Lefeber, 2001; Rysdyk, 2003; Skjetne & Fossen, 2001). For the latter approach, the Serret–Frenet frame (Micaelli & Samson, 1993; Samson, 1992) is often adopted to derive the error dynamics.

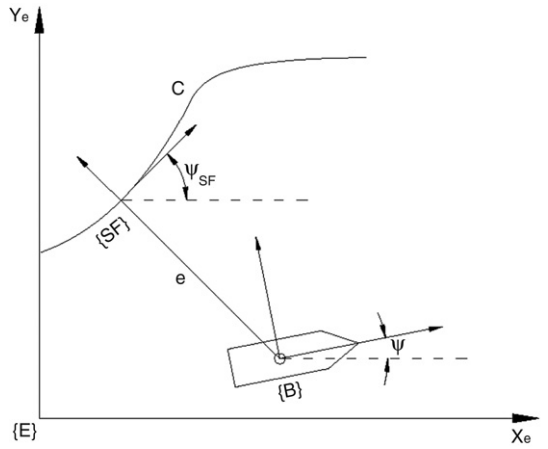

Fig. 1. Illustration of the coordinations in the earth frame (inertial frame) {E}, the ship body-fixed frame {B} and the Serret–Frenet frame {SF}.

Fig. 1 shows the Serret–Frenet frame used for path following control. The origin of the frame {SF} is located at the closest point on the curve C from the origin of frame {B}. The error dynamics based on the Serret–Frenet equations are introduced in Skjetne and Fossen (2001); they are given by

$$\begin{aligned}\dot{\bar{\psi}} &= \dot{\psi} - \dot{\psi}_{SF} \\ &= \frac{\kappa}{1-e\kappa}(u\sin\bar{\psi} - v\cos\bar{\psi}) + r, \end{aligned} \tag{1}$$

$$\dot{e} = u\sin\bar{\psi} + v\cos\bar{\psi}, \tag{2}$$

where e, defined as the distance between the origins of {SF} and {B}, and $\bar{\psi} := \psi - \psi_{SF}$, are referred to as the cross-track error and heading error respectively, and u, v, and r are the surge, sway, and yaw velocity respectively. ψ is the heading angle of the vessel and ψ_{SF} is the path tangential direction as shown in Fig. 1 (Skjetne & Fossen, 2001); κ is the curvature of the given path. The control objective of the path following problem is to drive e and $\bar{\psi}$ to zero.

For most path following problems for surface vessels in open sea, the path is a straight line or a way-point path, which consists of piecewise straight lines with the curvature κ being zero. Even if the desired path has non-zero curvature, it is often possible to approximate the curve by many piecewise straight lines. Therefore the heading error dynamics (1) can often be simplified as

$$\dot{\bar{\psi}} = r. \tag{3}$$

A marine surface vessel has total of six degrees of freedom. However, for path following, which seeks to control the ship in the horizontal plane, only three degrees of freedom, namely the surge u, sway v, and yaw r, are critical and the heave w, roll p, and pitch q are normally neglected. The most widely used ship model in path following research was developed in Fossen (1994); it is in the following form:

$$\dot{u} = \frac{m_{22}}{m_{11}}vr - \frac{d_{11}}{m_{11}}u + \frac{1}{m_{11}}u_1, \tag{4}$$

$$\dot{v} = -\frac{m_{11}}{m_{22}}ur - \frac{d_{22}}{m_{22}}v, \tag{5}$$

$$\dot{r} = \frac{m_{11}-m_{22}}{m_{33}}uv - \frac{d_{33}}{m_{33}}r + \frac{1}{m_{33}}u_2, \tag{6}$$

where the parameters $m_{ii} > 0$ are given by the ship's inertia and added mass effects. The parameters $d_{ii} > 0$ are given by the hydrodynamic damping. The available controls are the surge force u_1 and the yaw moment u_2.

Many different nonlinear design methodologies have been applied to the above model (4)–(6) (Breivik & Fossen, 2004a,b; Do & Pan, 2003; Do et al., 2002; Fossen et al., 2003; Jiang, 2002; Lefeber et al., 2003; Pettersen & Lefeber, 2001). However, due to the nonlinearities involved, the resulting control laws often have complex expressions, making the controller difficult for gain tuning and its performance sensitive to model parameters. In our work, the nonlinear model is used as a virtual ship for simulation and performance evaluation in Section 5. A more detailed 4-DoF container ship model and 2-DoF model boat with the assumption of a constant surge speed will serve as the controller test-bed. For the control design, however, the following reduced order linear model is used to facilitate the model-based approach:

$$\dot{v} = a_{11}v + a_{12}r, \tag{7}$$

$$\dot{r} = a_{21}v + a_{22}r + b_2\delta, \tag{8}$$

where a_{11}, a_{12}, a_{21}, a_{22}, b_1, and b_2 are constant parameters.

Remark 1. The 2-DoF linear model (7)–(8) is developed from the nonlinear 3-D0F model (4)–(6) based on the assumption that the surge velocity u is constant and the yaw moment u_2 is proportional to the rudder angle δ. In general, an independent control system is used to maintain the ship's surge speed. The constant surge velocity assumption is adopted by many researchers (Pettersen & Lefeber, 2001; Skjetne & Fossen, 2001). Notice that the rudder angle is the control input in the linear model (7)–(8), while the yaw moment is used as the input in (4)–(6). However, the former is a real actuator variable, but the latter is not.

The performance of the control system designed using the reduced order model will be presented to justify the use of the reduced order model when the same controller is applied to the full order model.

3. Controller design

Before proceeding to the controller design, an assumption could be made to further simplify the model and to avoid the underactuation problem. In ship maneuvering, the sway velocity is relatively small compared to other motion variables. Therefore we assume that the sway velocity is small enough to be neglected. With this assumption, the final model for control design, that captures the dominant ship maneuvering dynamics and path following error dynamics, with one control variable δ, has been simplified into

$$\dot{e} = u\sin\bar{\psi}, \tag{9}$$

$$\dot{\bar{\psi}} = r, \tag{10}$$

$$\dot{r} = a_{22}r + b_2\delta. \tag{11}$$

With u being treated as a constant, the dynamic system (9)–(11) assumes a triangular structure where the control action δ influences only r while r affects $\bar{\psi}$ and in turn $\bar{\psi}$ influences e. This triangular structure naturally renders the back-stepping control design (Krstic, Kanellakopoulos, & Kokotovic, 1995). However, given the nonlinearity of the dynamics and the "explosive nature" of the back-stepping design approach, the controller resulting from the standard back-stepping design approach involves many nonlinear terms (Skjetne & Fossen, 2001). As such, the controller may be susceptible to unmodeled dynamics and implementation errors.

In this work, in an attempt to enhance the system robustness and implementation ease, we propose a design approach that will result in a relatively simple control law. Instead of feedback linearization and nonlinearity cancelation, our back-stepping design is based on feedback dominance. The design procedure is delineated as follows:

Step 1:

Define the first Lyapunov function as

$$V_1 := \frac{1}{2}e^2 > 0. \tag{12}$$

Differentiating V_1 with respect to time yields

$$\dot{V}_1 = e\dot{e} = ue\sin\bar{\psi}. \tag{13}$$

Normally, according to the back-stepping design procedure, a virtual control of $\bar{\psi} = -\arcsin(c_1e)$ will be chosen to stabilize (9). However, this approach will result in a very complex controller when $\bar{\psi}$ is differentiated in the subsequent design steps. In our work, we choose the stabilizing virtual control $\alpha_1 := -c_1e, c_1 > 0$; then for $\bar{\psi} \in (-\pi, \pi)$, we have

$$\dot{V}_1 = -c_1ue^2\frac{\sin\bar{\psi}}{\bar{\psi}} + ue\frac{\sin\bar{\psi}}{\bar{\psi}}(\bar{\psi} - \alpha_1). \tag{14}$$

For $\bar{\psi} = \alpha_1$, we have

$$\dot{V}_1 = -c_1ue^2\frac{\sin\bar{\psi}}{\bar{\psi}} \le 0. \tag{15}$$

In deriving the inequality for V_1 in (15), we make use of the property $\sin(x)/x > 0, \forall x \in (-\pi, \pi)$.

Step 2:

Let $z_2 = \bar{\psi} - \alpha_1$ and differentiate it with respect to time; we obtain

$$\dot{z}_2 = \dot{\bar{\psi}} - \dot{\alpha_1} = r + c_1u\frac{\sin\bar{\psi}}{\bar{\psi}}(z_2 + \alpha_1). \tag{16}$$

Augment the first Lyapunov function into the second Lyapunov function as $V_2 := V_1 + \frac{p_1}{2}z_2^2 > 0$, where p_1 is a positive constant, whose role will become apparent in the subsequent analysis. Differentiating V_2 with respect to time yields

$$\begin{aligned}\dot{V}_2 &= e\dot{e} + p_1z_2\dot{z}_2 \\ &= -c_1ue^2\frac{\sin\bar{\psi}}{\bar{\psi}} + p_1z_2 \\ &\quad\times\left[r + c_1uz_2\frac{\sin\bar{\psi}}{\bar{\psi}} + \left(\frac{1}{p_1} - c_1^2\right)eu\frac{\sin\bar{\psi}}{\bar{\psi}}\right].\end{aligned} \tag{17}$$

If we select $p_1 = 1/c_1^2$, Eq. (17) becomes

$$\dot{V}_2 = -c_1ue^2\frac{\sin\bar{\psi}}{\bar{\psi}} + \frac{1}{c_1^2}z_2\left[r + c_1uz_2\frac{\sin\bar{\psi}}{\bar{\psi}}\right]. \tag{18}$$

Remark 2. Note that the introduction of p_1 in V_2 allow us to eliminate the cross-product term in $\dot{V}_2$ that involves nonlinearity. Without this flexibility in V_2, one has to rely on the virtual control to cancel the nonlinear term to achieve $\dot{V}_2 \le 0$. It should be noted that, since both c_1 and p_1 are design parameters and no model parameters are involved in meeting the condition $p_1 = 1/c_1^2$, Eq. (18) is not subject to modeling errors.

To design the next virtual control for the (e, z_2) dynamics, we use feedback dominance instead of feedback linearization (which will involve the exact cancelation of nonlinearities) to form the stabilizing virtual control. By selecting $\alpha_2 := -c_2z_2$ and making c_2 satisfy $c_2 > c_1u$, we have

$$\dot{V}_2 = -c_1ue^2\frac{\sin\bar{\psi}}{\bar{\psi}} - \frac{c_2}{c_1^2}z_2^2\left[1 - \frac{c_1u}{c_2}\frac{\sin\bar{\psi}}{\bar{\psi}}\right] + \frac{1}{c_1^2}z_2(r - \alpha_2). \tag{19}$$

If $r = \alpha_2$, we have

$$\dot{V}_2 = -c_1 u e^2 \frac{\sin\bar{\psi}}{\bar{\psi}} - \frac{c_2}{c_1^2} z_2^2 \left[1 - \frac{c_1 u}{c_2}\frac{\sin\bar{\psi}}{\bar{\psi}}\right] \le 0, \tag{20}$$

where the inequality in (20) is a direct result of $c_2 > c_1 u$ and $0 < \sin(\bar{\psi})/\bar{\psi} < 1$. Note that, in (20), we use the linear virtual control $-c_2 z_2$ to dominate, instead of cancel, the nonlinear term, thus the name "feedback dominance".

Step 3:

Define $z_3 = r - \alpha_2$ and differentiate it with respect to time; we obtain

$$\dot{z_3} = \dot{r} - \dot{\alpha_2} = a_{22} r + b_2 \delta - \dot{\alpha_2}. \tag{21}$$

Further augmenting the second Lyapunov function as $V_3 := V_2 + \frac{p_2}{2} z_3^2 > 0$, where p_2 is a positive constant, we have

$$\begin{aligned}\dot{V}_3 = {} & -c_1 u e^2 \frac{\sin\bar{\psi}}{\bar{\psi}} - \frac{c_2}{c_1^2} z_2^2 \left[1 - \frac{c_1 u}{c_2}\frac{\sin\bar{\psi}}{\bar{\psi}}\right] \\ & + p_2 z_3 \left[\frac{1}{c_1^2 p_2} z_2 + a_{22} r + b_2 \delta - \dot{\alpha_2}\right].\end{aligned} \tag{22}$$

If we select

$$\delta = \frac{1}{b_2}\left(-c_3 z_3 - \frac{1}{c_1^2 p_2} z_2 - a_{22} r + \dot{\alpha_2}\right), \tag{23}$$

then (22) turns into

$$\begin{aligned}\dot{V}_3 = {} & -c_1 u e^2 \frac{\sin\bar{\psi}}{\bar{\psi}} - \frac{c_2}{c_1^2} z_2^2 \left[1 - \frac{c_1 u}{c_2}\frac{\sin\bar{\psi}}{\bar{\psi}}\right] - p_2 c_3 z_3^2 \\ \le {} & 0,\end{aligned} \tag{24}$$

and the second inequality holds if $\bar{\psi} \in (-\pi, \pi)$ and $c_2 > c_1 u$. Furthermore, $\dot{V}_3 = 0$ only if $(e, z_2, z_3) = (0, 0, 0)$, which means that the control law (23) renders the system (9), (10), (11) to be asymptotically stable.

Substituting the expressions for z_2, z_3, and $\dot{\alpha_2}$ in terms of the original states, (23) becomes

$$\delta = -\bar{c}_1 e - \bar{c}_2 \bar{\psi} - \bar{c}_3 r - \bar{c}_4 u \sin\bar{\psi}, \tag{25}$$

where

$$\bar{c}_1 = \frac{1}{b_2}\left(c_1 c_2 c_3 + \frac{1}{c_1 p_2}\right), \tag{26}$$

$$\bar{c}_2 = \frac{1}{b_2}\left(c_2 c_3 + \frac{1}{c_1^2 p_2}\right), \tag{27}$$

$$\bar{c}_3 = \frac{a_{22} + c_2 + c_3}{b_2}, \tag{28}$$

$$\bar{c}_4 = \frac{c_1 c_2}{b_2}. \tag{29}$$

As shown in Eq. (25), the final control law has a very simple structure. The first three terms in the control law are linear and the only nonlinearity comes from the last term.

Remark 3. Besides their functions as mentioned in Remark 2, namely, to eliminate the nonlinear term in the design procedure and therefore simplify the resulting control, the parameters p_1 and p_2 also serve to normalize the effects of different variables in the Lyapunov function. For example, the three variables in V_3 are e, $z_2 = \psi - \alpha_1$, and $z_3 = r - \alpha_2$, which have the order of magnitude of 1000, π, and 0.01, respectively, in the case of the 4-DoF container ship. Thus, p_1 and p_2 should have the order of 10^5 and 10^{11} to make all three variables have comparable influences on the V_3.

In contrast, nonlinear control designed using the standard back-stepping and feedback linearization, instead of "feedback dominance", would have the form (30):

$$\delta = -\frac{1}{b_2}(k_3 \bar{z}_3 + \cos(\arcsin(\bar{z}_2 + \beta_1))\bar{z}_2 + a_{22} r - \dot{\beta}_2), \tag{30}$$

where

$$\beta_1 = -k_1 e, \tag{31}$$

$$\bar{z}_2 = \sin\bar{\psi} - \beta_1, \tag{32}$$

$$\beta_2 = \frac{-ue - k_2 \bar{z}_2 + \dot{\beta}_1}{\cos(\arcsin(\bar{z}_2 + \beta_1))}, \tag{33}$$

$$\bar{z}_3 = r - \beta_2, \tag{34}$$

and k_1, k_2 and k_3 are positive control parameters. When $\bar{z}_2$, $\bar{z}_3$, β_1, and $\dot{\beta}_2$ are substituted by their corresponding expressions in terms of the original states, the control law (30) becomes

$$\begin{aligned}\delta = {} & -\frac{1}{b_2}[(a_{22} + k_1 u + k_2 + k_3) r + (k_1 u + k_2) r \tan^2\bar{\psi} \\ & + (k_3 u + k_1 k_2 k_3) e \sec\bar{\psi} + (u + k_1 k_2) e r \sin\bar{\psi} \sec\bar{\psi} \\ & + (u^2 + k_1 k_2 u + k_2 k_3 - k_1 k_3 u) \tan\bar{\psi} \\ & + \sin\bar{\psi}\cos\bar{\psi} + k_1 e \cos\bar{\psi}].\end{aligned} \tag{35}$$

The resulting control law (35) has a lengthy expression comprising many nonlinear terms, most of which are due to the non-affine function of the input that the feedback design is trying to cancel. This complexity will not only make the controller difficult to tune, but also makes it susceptible to implementation errors and model uncertainties.

Remark 4. Note that the controller (25) has proportional, integral, and derivative terms when e and r are expressed in terms of $\bar{\psi}$; the tuning of the controller gains is relatively easy in the sense that the effects of each parameter on the system dynamics and control saturation can be interpreted in physical variables and many of the PID tuning algorithms can be used.

4. Robustness analysis

In deriving the path following controller, the linear vessel model was used and the sway velocity was neglected. To incorporate the nonlinearities and non-zero sway velocities, we use the following model in our robustness analysis:

$$\dot{e} = u \sin\bar{\psi} + v \cos\bar{\psi}, \tag{36}$$

$$\dot{\bar{\psi}} = r, \tag{37}$$

$$\dot{r} = a_{21} v + a_{22} r + b_2 \delta + \Delta, \tag{38}$$

where Δ captures the unmodeled dynamics.

For the uncertainties Δ, we assume:

A1. There exist positive constants γ_0, γ_v, and γ_r such that

$$|\Delta| \le \gamma_0 + \gamma_v |v| + \gamma_r |r|. \tag{39}$$

For the sway dynamics, which is not considered in the controller design, we make the following assumption:

A2. There exist positive constants $\bar{\gamma}_0$ and $\bar{\gamma}_r$ such that

$$|v| \le \bar{\gamma}_0 + \bar{\gamma}_r |r|. \tag{40}$$

Remark 5. Comparing (8) with the nonlinear yaw dynamical equation (6) and assuming $a_{22} = -\frac{d_{33}}{m_{33}}$, we have

$$\Delta = \left(\frac{m_{11} - m_{22}}{m_{33}} u - a_{21}\right) v + \frac{1}{m_{33}} u_2 - b_2 \delta. \tag{41}$$

Given the constant surge speed assumption, the term $\frac{m_{11} - m_{22}}{m_{33}} u - a_{21}$ is zero. However, in the actual maneuvering, the varying

surge speed will lead to non-zero values for $\frac{m_{11}-m_{22}}{m_{33}}u - a_{21}$. Therefore, γ_v is introduced to capture these surge speed effects and other parameter uncertainties. On the other hand, the assumption that the yaw moment induced by the rudder action is proportional to the rudder angle is an approximation for the ship's physical responses observed in simulations of high fidelity models and experiments. Recognizing that the rudder induced yaw moment also depends on the ship's state such as u, v and r, we introduce the γ_0 term to capture the higher order but bounded nonlinear terms in the control input (the difference between $b_2\delta$ and $\frac{1}{m_{33}}u_2$) and other model dynamics. Furthermore, the effects of parameter uncertainties in the r term are captured by γ_r.

Remark 6. For a surface vessel maneuvering in calm water, the non-zero rudder angle, which is the only control input considered here, will result in corresponding non-zero sway velocity v and yaw rate r. Normally, the magnitudes of v and r are both related to the magnitude of the rudder angle. Extensive simulation using a high order nonlinear model shows that there exists a phase lag between the response v and r. Therefore, we use $\bar{\gamma}_0$ in A2 to capture this lag and $\bar{\gamma}_r$ for the proportional relation between v and r.

To study the stability of the closed loop system with the proposed controller implemented to the system (36)–(38), the Lyapunov function V_3 used in the controller derivation in the previous section is adopted. Differentiating V_3 with respect to time, we obtain

$$\begin{aligned}\dot{V}_3 = {} & -c_1 u e^2 \frac{\sin\bar{\psi}}{\bar{\psi}} - \frac{c_2}{c_1^2} z_2^2 \left[1 - \frac{c_1 u}{c_2}\frac{\sin\bar{\psi}}{\bar{\psi}}\right] - p_2 c_3 z_3^2 \\ & + ve\cos\bar{\psi} + \frac{1}{c_1} v z_2 \cos\bar{\psi} + p_2 c_1 c_2 v z_3 \cos\bar{\psi} \\ & + p_2 a_{21} v z_3 + p_2 z_3 \Delta. \end{aligned} \tag{42}$$

Define $d_1 := c_1 u \frac{\sin\bar{\psi}}{\bar{\psi}}$, $d_2 := \frac{c_2}{c_1^2}(1 - \frac{c_1 u}{c_2}\frac{\sin\bar{\psi}}{\bar{\psi}})$, and $d_3 := p_2 c_3$; it follows from (42) that

$$\begin{aligned}\dot{V}_3 \le {} & -d_1 e^2 - d_2 z_2^2 - d_3 z_3^2 \\ & + |v|(|\cos\bar{\psi}||e| + \frac{|\cos\bar{\psi}|}{c_1}|z_2| + p_2 c_1 c_2 |\cos\bar{\psi}||z_3| \\ & + p_2|a_{21}||z_3|) + p_2|z_3||\Delta|. \end{aligned} \tag{43}$$

If A1 and A2 are satisfied, and noticing that $|r| \le |z_3| + c_2|z_2|$, (43) leads to

$$\begin{aligned}\dot{V}_3 \le {} & -d_1 e^2 - d_2 z_2^2 - d_3 z_3^2 + l_1|e| + l_2|z_2| + l_3|z_3| + n_1 z_2^2 + n_2 z_3^2 \\ & + q_1|e||z_2| + q_2|e||z_3| + q_3|z_2||z_3|, \end{aligned} \tag{44}$$

where

$$l_1 = \bar{\gamma}_0|\cos\bar{\psi}|, \tag{45}$$

$$l_2 = \frac{\bar{\gamma}_0|\cos\bar{\psi}|}{c_1}, \tag{46}$$

$$l_3 = p_2(c_1 c_2 \bar{\gamma}_0|\cos\bar{\psi}| + \bar{\gamma}_0|a_{21}| + \gamma_0 + \bar{\gamma}_0\gamma_v), \tag{47}$$

$$n_1 = \frac{c_2\bar{\gamma}_r|\cos\bar{\psi}|}{c_1}, \tag{48}$$

$$n_2 = p_2(c_1 c_2 \bar{\gamma}_r|\cos\bar{\psi}| + \bar{\gamma}_r|a_{21}| + \gamma_r + \bar{\gamma}_r\gamma_v), \tag{49}$$

$$q_1 = c_2\bar{\gamma}_r|\cos\bar{\psi}|, \tag{50}$$

$$q_2 = \bar{\gamma}_r|\cos\bar{\psi}|, \tag{51}$$

$$q_3 = p_2 c_2(c_1 c_2\bar{\gamma}_r|\cos\bar{\psi}| + |a_{21}|\bar{\gamma}_r + \bar{\gamma}_r\gamma_v + c_1\gamma_r) + \frac{c_3\bar{\gamma}_r}{c_1}. \tag{52}$$

Using the arithmetic-mean–geometric-mean inequality in (44), we have

$$\dot{V}_3 \le -\bar{d}_1 e^2 - \bar{d}_2 z_2^2 - \bar{d}_3 z_3^2 + l_1|e| + l_2|z_2| + l_3|z_3|, \tag{53}$$

where

$$\bar{d}_1 = d_1 - \frac{q_1}{2} - \frac{q_2}{2}, \tag{54}$$

$$\bar{d}_2 = d_2 - n_1 - \frac{q_1}{2} - \frac{q_3}{2}, \tag{55}$$

$$\bar{d}_3 = d_3 - n_2 - \frac{q_2}{2} - \frac{q_3}{2}. \tag{56}$$

From (53), it follows that the system will converge to a region around the origin that is characterized by $\{(e, z_2, z_3) \mid |e| \le \frac{l_1}{\bar{d}_1}, |z_2| \le \frac{l_2}{\bar{d}_2}, |z_3| \le \frac{l_3}{\bar{d}_3}\}$. By a proper selection of the controller gains c_1, c_2, c_3, and p_2, we can make the region very small if there is no significant unmodeled dynamics, which means γ_0, γ_v, and γ_r are small, and the sway velocity is relatively small, which means $\bar{\gamma}_0$ and $\bar{\gamma}_r$ are small.

Remark 7. In order to eliminate the steady state error in cross-track error e when environmental disturbances exist (such as a lateral current), we could design a controller with an integral term e by augmenting the system dynamics (9)–(11) with $\dot{e}_I = e$, where e_I is the integral of the cross-track error e. However, the feedback dominance technique for simplifying the back-stepping controller is not applicable in this case. Thus, the resulting controller derived by following the standard back-stepping technique is very complex, which defeats our purpose to develop a simple controller for easy gain-tuning and analysis. In fact, an integral term $-\bar{c}_4 e_I$ ($\bar{c}_4$ is the positive gain) could be directly added into the control law (25) to achieve good performance with environmental disturbances. However, rigorous analysis would be difficult to establish stability and converging performance in this case.

5. Simulation results

A mathematical model for a single-screw high-speed container ship (often referred to as S175 in the marine engineering community) with four degrees of freedom (surge, sway, roll, and yaw) has been presented in Fossen (1994). This 4-DoF ship dynamical model is highly nonlinear with 10 states and 2 control inputs: $X = [u, v, r, p, x, y, \psi, \phi, n, \delta]$, and $U = [n_c, \delta_c]$. u, v, r, and p are the surge velocity, sway velocity, yaw rate, and roll rate with respect to the ship-fixed frame, respectively; the corresponding displacements with respect to the inertial frame (fixed on the earth with North and East definition) are denoted as x, y, ψ, and ϕ, the propeller shaft speed as n, the rudder angle as δ, and n_c and δ_c are the commands for the propeller speed and rudder angle, respectively. The actuator input saturation and rate limits are also incorporated in this model. The 4-DoF nonlinear model is one of the most comprehensive ship models available in open literature. It captures the fundamental characteristics of the ship dynamics and offers satisfactory accuracy over a wide range of operating conditions in open-loop simulations.

To verify and illustrate the theoretical results, the proposed control law is implemented and simulated with the above 4-DoF nonlinear container model along with the corresponding reduced order model. The actuator saturation and its rate limits ($|\delta| \le$ 20 deg and $|\dot{\delta}| \le$ 5 deg/s) are incorporated in the performance evaluations. In the simulations, $u = 7$ m/s, $a_{22} = -0.10676$ and $b_2 = 0.0028385$. Different controller gains are used to achieve different transient performance; the numerical values of the gains used for simulations are listed in Table 1. Notice that the large value assumed by p_2 is used to normalize the variables in the Lyapunov function.

The effects of the controller gains on the dynamic response are first illustrated in Fig. 2. The controller with gain3 (corresponding to the largest c_1) has the fastest convergent speed. This response

Table 1
Controller gains for simulation.

	c_1	c_2	c_3	p_2
gain1	0.0005	0.2	0.005	10^{11}
gain2	0.001	0.2	0.006	10^{11}
gain3	0.006	0.2	0.008	10^{11}

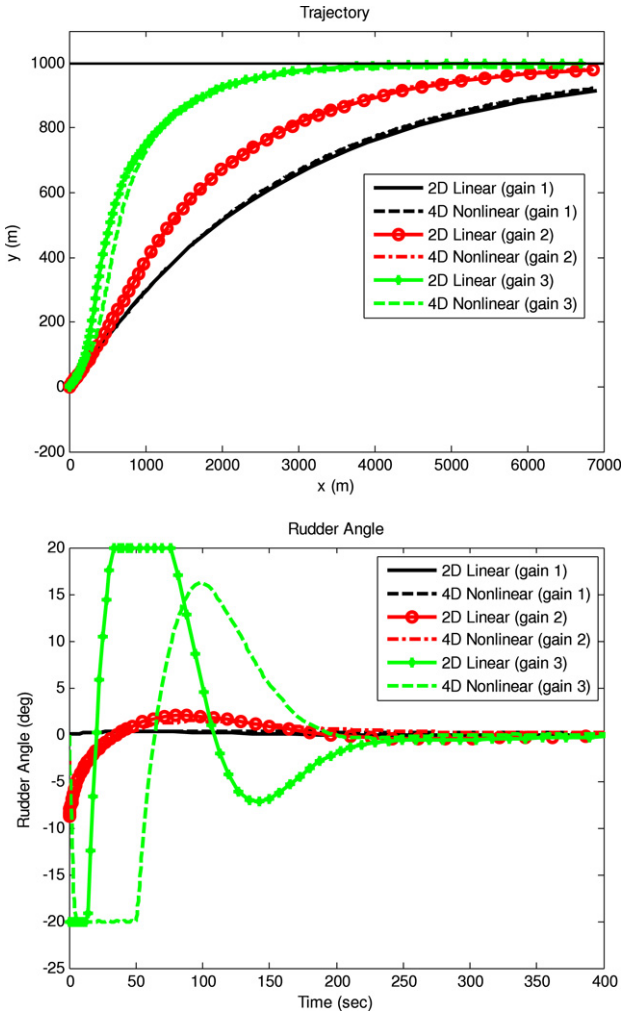

Fig. 2. Simulation results of the ship response with different control gains.

speed, however, is achieved at the expense of large rudder angle and actuator saturation. From Fig. 2 (where the legends linear and nonlinear indicate the response of the linear model and the nonlinear model, respectively), one can also see that the response of the linear model is in excellent agreement with that of the nonlinear model. This demonstrates the robustness of the control law against potential modeling errors.

The control algorithm is also tested with different initial conditions; see Fig. 3. The ship is placed with initial heading angles −5, −45, and 15 [deg] and cross-track errors 100, 500, and 1000 [m] respectively. The initial v and r are set to zero. Fig. 3 shows that the controller (with gain2) is capable of achieving path following for all the initial conditions tested. It is also shown that the rudder angle and the convergent rate depend in general on the magnitude of the initial errors, which verifies the nonlinear nature of the underlying dynamics.

To evaluate the robustness of the control system, additional uncertainties, such as time delays and measurement noises, are considered. A time delay (1 s and 5 s) is introduced in the control execution, while the measurement noise (white noise with

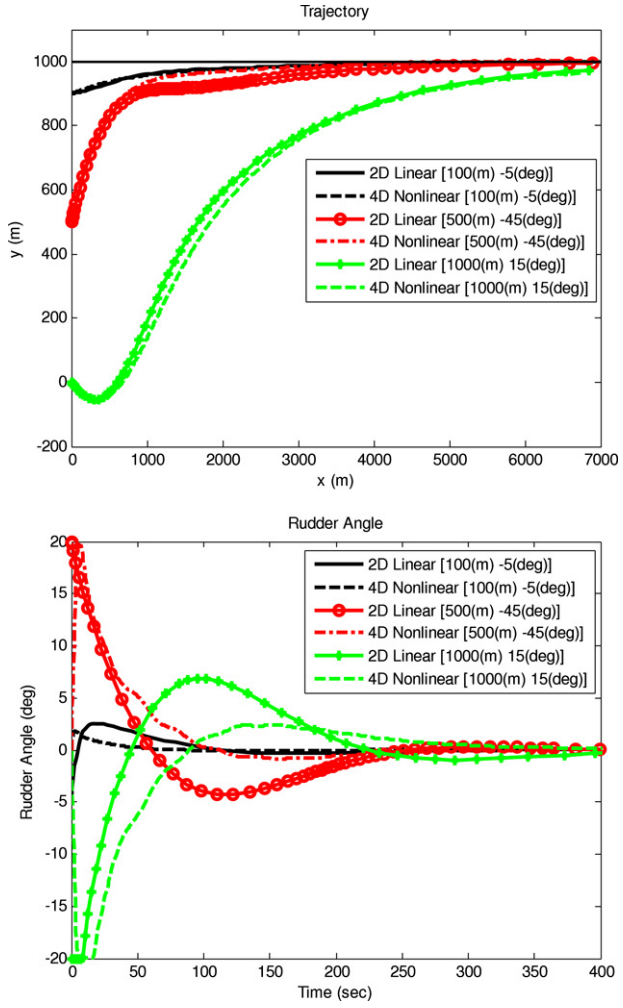

Fig. 3. Simulation results of the control system for different initial conditions (the numbers in brackets are the initial cross-track error and heading error).

standard deviation of $p|S|$ with p being the noise factor and S being the order of the magnitude of the measured signal) is introduced for all the signals (e, $\bar{\psi}$, and r) used in the control implementation. Figs. 4 and 5 show the simulation results of the vessel response in the presence of time delay and measurement noise, respectively (both with gain2). One can see that while the path following performance is almost unaffected by these adversary factors in both cases, these uncertainties introduce oscillations in the rudder responses.

Furthermore, we compared the LQR, feedback dominance backstepping controller (FDBS), and linearized FDBS controllers by simulations. The LQR controller is designed based on the linearized version of system (9)–(11) (which is also referred to as the Nomoto model in Fossen (2002)) and the linearized FDBS is developed by replacing $\sin\bar{\psi}$ with $\bar{\psi}$ in (25). To get the best path following performance in terms of the fast convergence speed and overshoot avoidance, we tuned the controller gains for both the LQR and the FDBS controllers carefully. The Q and R matrices employed in the LQR controller are $[0.018^2, 0, 0; 0, 3.5^2, 0; 0, 0, 0]$ and 1 respectively. The gains adopted in the FDBS and linearized FDBS controllers are $c_1 = 0.0028$, $c_2 = 0.1$, $c_3 = 0.1$, and $p_2 = 10^{11}$. The simulation results for the three different controllers are shown in Fig. 6. It can be seen from Fig. 6 that the FDBS controller achieves the fastest path following convergence speed with the least rudder actions, while the LQR controller has slower path following and more rudder actions than the FDBS controller. We also notice that

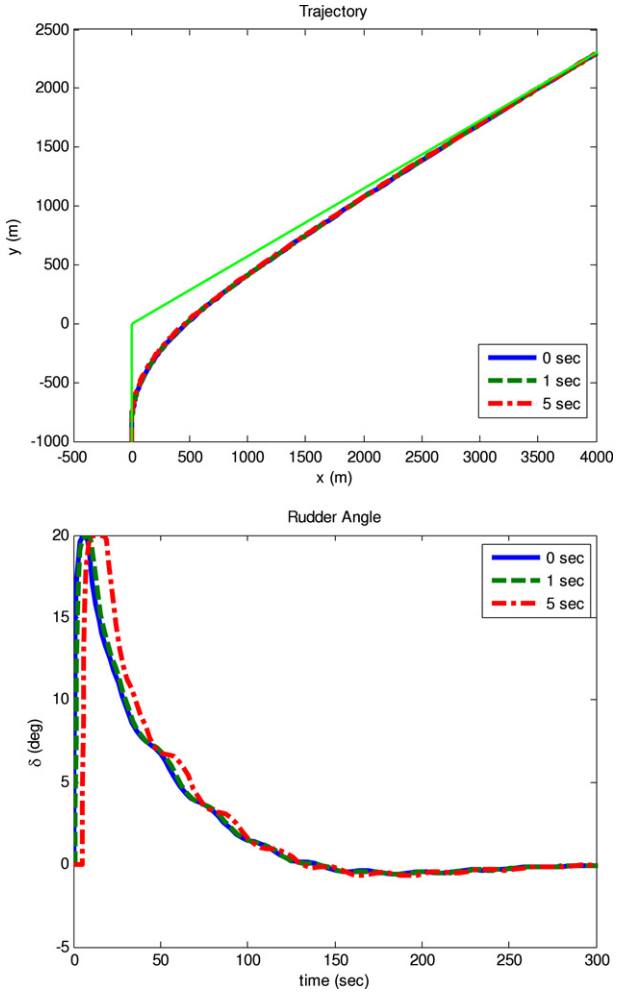

Fig. 4. Simulation results with time delay.

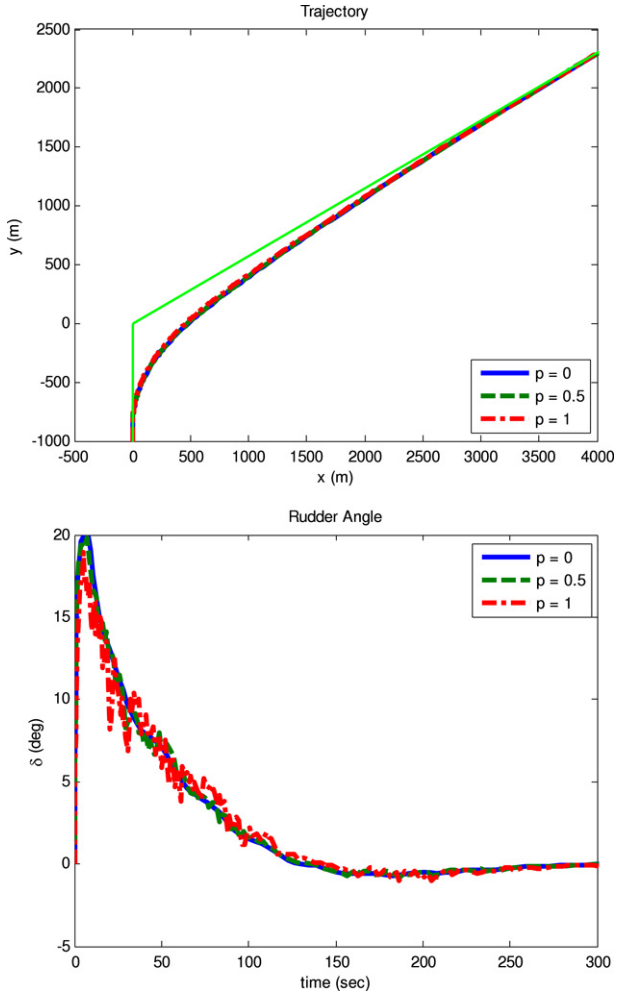

Fig. 5. Simulation results with measurement noises.

the linearized FDBS controller has a slight overshoot in both cross-track and heading errors.

To further verify the controller performance and prepare for the experimental validation, the numerical simulations of a model boat (the details of this boat will be given in Section 6) with the controller proposed in this paper are conducted. The numerical model of the model boat has two degrees of freedom, sway and yaw, by assuming that the surge velocity is constant. In these simulations, the gains of the controller are set to $c_1 = 0.35$, $c_2 = 0.5$, $c_3 = 10$, and $p_2 = 10\,000$. The values of c_1, c_2, and c_3 used here are much bigger and that of p_2 is much smaller than the ones in Table 1. The difference is due to the different scales used in the two applications. Fig. 7 shows that path following is achieved as all the path following errors are going to zero for all the initial conditions tested.

6. Experimental results

6.1. Experimental platform

To support the control development, a fully instrumented model ship is designed so that the control algorithm developed in Section 3 can be experimentally evaluated. The model ship is actuated with two contra-rotating main propellers and two rudders aft. The propellers and rudders are actuated by two DC servo motors fitted with encoders and tachometers, respectively. The main parameters of the model ship are given in Table 2. The two ship parameters a_{22} and b_2, which are the only parameters needed for the controller design, have the values of -0.2841 and 0.1316, respectively.

Table 2
Principal particulars of the model ship.

Item	Symbol	Value
Length	L	1.60 m
Breadth	B	0.38 m
Height	H	0.17 m
Mass	m	38 kg
Inertia	I_z	2.7 kg m^2

When the model ship is tested in the towing tank (320 ft $\times$ 22 ft $\times$ 10.5 ft) located in the Marine Hydrodynamics Laboratories (MHL) of the University of Michigan, the GPS signals are not available (even if they are available, the accuracy of GPS signals is not high enough for the model test), four infra-red cameras are used, in lieu of the GPS system, to provide the feedback signal to the control system. A picture of the instrumented model is shown in Fig. 8.

Real-time feedback control is accomplished using PC-based PC104 hardware which runs the QNX real-time operating system. PC104 communicates, through a wireless LAN, to a host PC, on which the control algorithm is programmed and tuned, the data acquisition function is performed, and the ship's position signals are collected from the camera system and transmitted to PC104. The key control and communication devices are shown in Fig. 9, together with the connections among the devices.

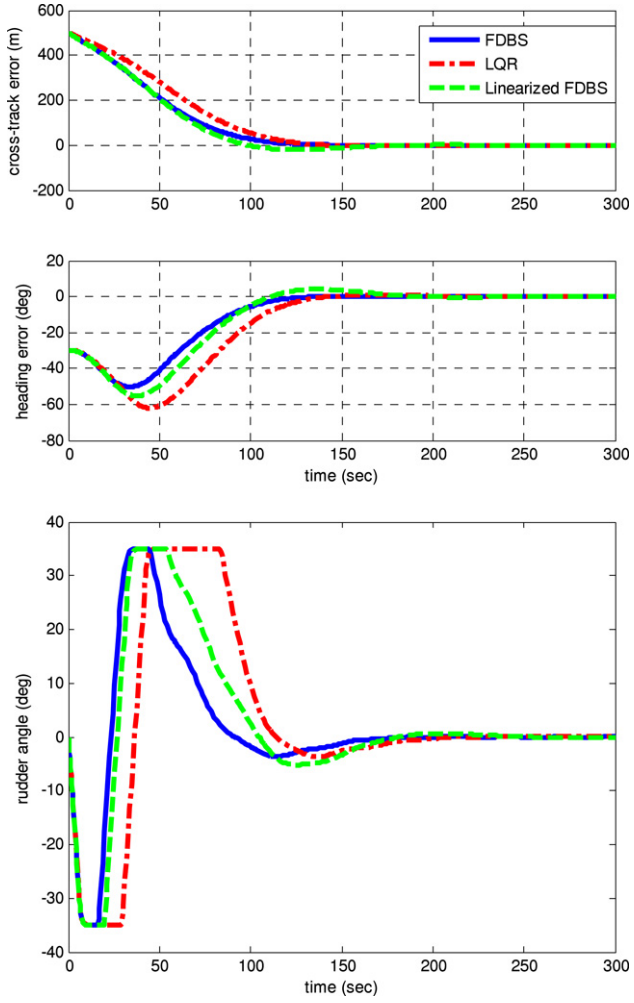

Fig. 6. Comparison of simulation results of the FDBS, LQR, and linearized FDBS controllers.

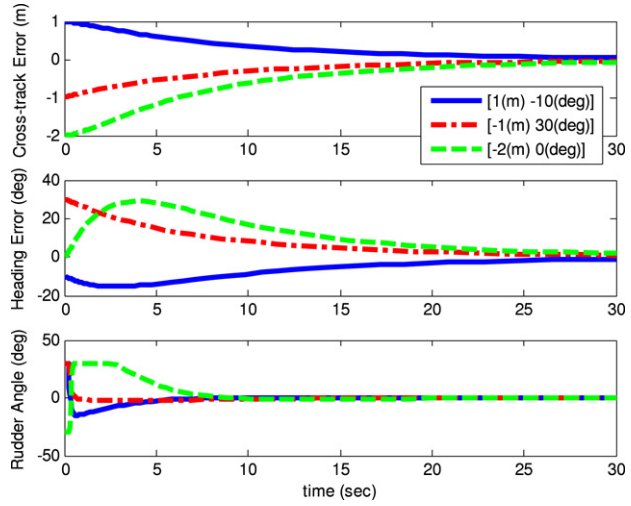

Fig. 7. Simulation results of the model boat for different initial conditions (the numbers in brackets are the initial cross-track error and heading error).

6.2. Experimental results

For the experimental validation, the on-board computer controls and coordinates the motion of the two propeller motors and the two rudder motors according to the control algorithm. At the higher level, the desired path to be tracked is specified and communicated wirelessly to the on-board controller. In the MHL towing tank where the experiments were conducted, the speed of the towing carriage (on which the camera position tracking system is mounted) and the ship's position data captured by the camera motion tracking system are transmitted in real time to PC104 through two pairs of wireless RF modems. The actuators have their low level inner loop control for the propeller speed and the rudder angle. PI controllers with the gains $K_{prop} = (0.05, 1.0)$ and $K_{rudder} = (3, 5)$ are used. The control system runs at a sample rate of 1 ms. In the experiments, the same controller parameters used in the simulation are downloaded to the on-board processor.

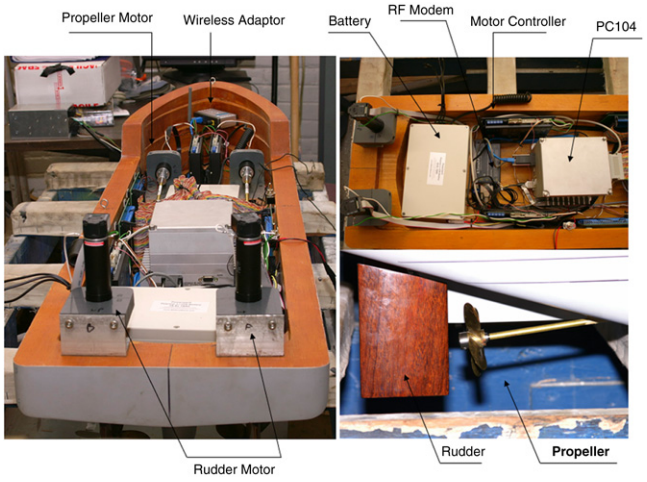

Fig. 8. A system overview of the fully instrumented model ship.

The initial conditions of the model ship are not specified. Instead, the boat is first running in the manual mode where the operator is trying to position the ship to the launching area. Then the system is switched to the autonomous mode where the rudders are controlled according to the algorithm specified in Section 3. In our first test, the control algorithm is tested with a constant propeller speed of 300 rpm, and the rudder is constrained to turn only ± 30 deg to prevent potential mechanical damage to the model ship.

In all experiments, the model ship could converge to the desired path, regardless of where it actually started in the towing tank. Fig. 10 shows one example of the experiment results, giving the time evolution of the states y, $\bar{\psi}$, and the rudder angle δ. The first and second plots given in Fig. 10 show that the ship tracks the path well given that the cross-track and heading errors are intended to approach zero. The control algorithm is also validated to be effective under other different propeller speeds.

Fig. 10 also shows the comparison between the simulation and experimental validation results of the model boat. Although the heading error response matches well, there are noticeable discrepancies in the cross-track error and rudder responses between simulation and experimental results. The simulation result tends to correct the cross-track error faster than the experimental result. We found that this is mainly due to the fact that there exists a surge speed reduction in experiments when the boat is making a turn, while in simulations a constant speed assumed. Analysis of the speed data reveals that, for this model ship, a large enough ship speed reduction (about 15%–20%) results from the maneuvering motion, when the propeller speed is kept constant. To verify the explanation, we simulated a boat with a reduced surge speed (reduced to 0.51 m/s from 0.62 m/s) and summarized the results in the Fig. 11, which shows a much better match between the cross-track error of the simulation and experimental results. In Fig. 11, the simulation result is shown to have less rudder effort than the experimental results, and this error could be attributed to the measurement bias in the rudder angle detection sensor. This error tends to be small for the initial phase of the experiments. It expands over time as the error accumulates, and disappears after the sensor

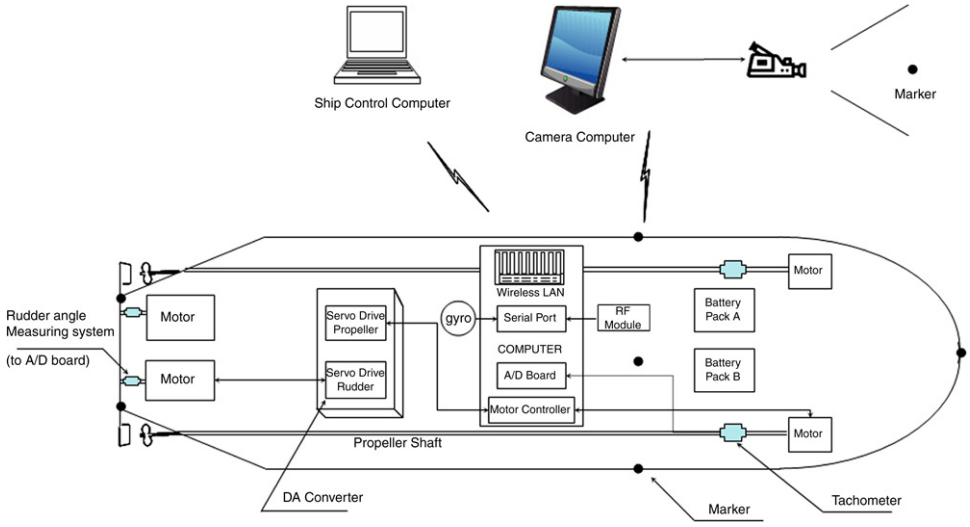

Fig. 9. Wireless link between devices.

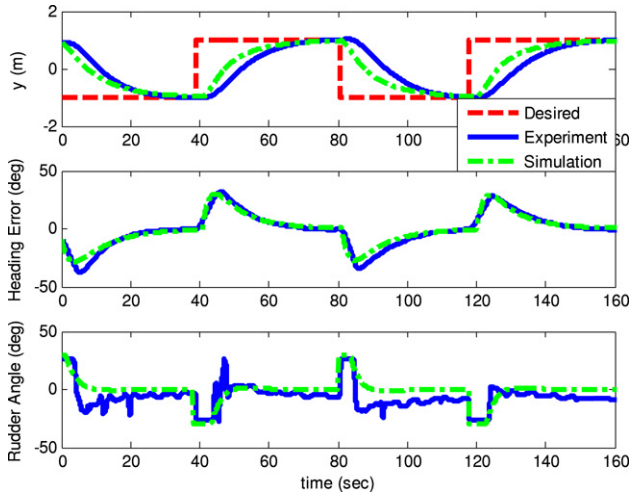

Fig. 10. Comparison of simulation and experiment results.

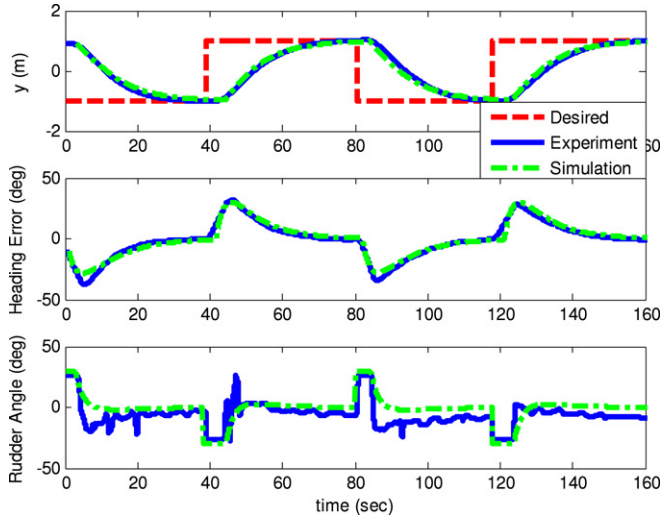

Fig. 11. Comparison of simulation (with a reduced surge speed) and experiment results.

reset. Furthermore, the model uncertainties, environmental disturbance, and implementation delay and error might all contribute to the discrepancies between the simulation and experiment results.

7. Conclusions

In this paper, we propose a control system for marine surface vessel path following. The back-stepping design, together with feedback dominance, leads to a simple control law that achieves asymptotic path following. Robustness analysis against unmodeled dynamics was also performed. Simulation results revealed that the controller enhanced the path following capability while demonstrating robust performance against model uncertainties, communication delays, and measurement noise. The efficacy of the designed controller was also validated by successful experimental results.

References

Breivik, M., & Fossen, T. I. (2004a). Path following for marine surface vessels. *MTTS/IEEE TECHNO-OCEAN*, *4*, 2282–2289.

Breivik, M., & Fossen, T.I. (2004b). Path following of straight lines and circles for marine surface vessels. In *Proceeding of the 6th IFAC CAMS*.

Breivik, M., & Fossen, T. I. (2005). Principles of guidance-based path following in 2d and 3d. In *44th IEEE conference on decision and control* (pp. 627–634).

Do, K. D., & Pan, J. (2003). Global tracking control of underactuated ships with off-diagonal terms. In *Proceedings of the 42nd IEEE conference on decision and control* (pp. 1250–1255).

Do, K. D., & Pan, J. (2006). Underactuated ships follow smooth paths with integral actions and without velocity measurements for feedback: Theory and experiments. *IEEE Transactions on Control Systems Technology*, *14*(2), 308–322.

Do, K. D., Jiang, Z. P., & Pan, J. (2002). Underactuated ship global tracking under relaxed conditions. *IEEE Transactions on Automatic Control*, *47*, 1529–1536.

Do, K. D., Jiang, Z. P., & Pan, J. (2004). Robust adaptive path following of underactuated ships. *Automatica*, *40*, 929–944.

Encarnacao, P., & Pascoal, A. (2001). Combined trajectory tracking and path following for marine vehicles. In *Proceeding 9th Mediterranean conference on control and automation*.

Fossen, T. I. (1994). *Guidance and control of ocean vehicles*. John Wiley and Sons, Inc.

Fossen, T. I. (2002). *Marine control systems*. Marine Cybernetics.

Fossen, T. I., Breivik, M., & Skjetne, R. (2003). Line-of-sight path following of underactuated marine craft. In *Proceeding of the sixth IFAC conference maneuvering and control of marine crafts* (pp. 244–249).

Holzhuter, T. (1997). Lqr approach for the high-precision track control of ships. *IEEE Proceedings of Control Theory and Applications*, *144*(2), 121–127.

Jiang, Z. P. (2002). Global tracking control of underactuated ships by Lyapunov's direct method. *Automatica*, *38*, 301–309.

Kallstrom, C. G. (2000). Autopilot and track-keeping algorithms for high-speed craft. *Control Engineering Practice*, *8*(2), 185–190.

Krstic, M., Kanellakopoulos, I., & Kokotovic, P. V. (1995). *Nonlinear and adaptive control design*. John Wiley and Sons, Inc.

Lapierre, L., Soetanto, D., & Pascoal, A. (2003). Nonlinear path following with applications to the control of autonomous underwater vehicles. In *Proceeding 42nd IEEE conference on decision and control* 2 (pp. 1256–1261).

Lefeber, E., Pettersen, K. Y., & Nijmeijer, H. (2003). Tracking control of an underactuated ship. *IEEE Transactions on Control Systems Technology*, *11*, 52–61.
Li, Z., Sun, J., & Oh, S. (2007). A robust nonlinear control design for path following of a marine surface vessel. *IFAC conference on control applications in marine systems*.
Micaelli, A., & Samson, C. (1993). Path following and time varying feedback stabilization of a wheeled mobile robot. *Technical report*. INRIA.
Pettersen, K. Y., & Lefeber, E. (2001). Way-point tracking control of ships. In *Proceeding of 40th IEEE conference decisions and control*.
Pettersen, K. Y., & Nijmeijer, H. (1998). Tracking control of an underactuated surface vessels. In *Proceeding of 37th IEEE conference decisions and control*.
Rysdyk, R. (2003). Uav path following for constant line-of-sight. In *Proceeding of the 2nd AIAA*.
Samson, C. (1992). Trajectory tracking for unicycle type and two steering wheels mobile robots. In *Proceedings of ICARV* pp. RO–13.1.
Skjetne, R., & Fossen, T. I. (2001). Nonlinear maneuvering and control of ships. In *Proceeding of the MTS/IEEE OCEANS*.
Skjetne, R., Fossen, T. I., & Kokotovic, P. V. (2004). Robust output maneuvering for a class of nonlinear systems. *Automatica*, *40*, 373–383.

Zhen Li was born in Zhejiang, China, in 1980. He received his B.Eng. and M.Eng. degrees in 2001 and 2004, respectively, both from Shanghai Jiao Tong University, China. He also received his M.S.E. degree in Electrical Engineering: System in 2008 from University of Michigan, Ann Arbor, USA. He is currently a Ph.D. candidate and graduate research assistant in the Department of Naval Architecture and Marine Engineering, University of Michigan. His research interests include modeling and control of marine systems.

Jing Sun received her Ph.D. degree from the University of Southern California in 1989, and her B.S. and M.S. degrees from University of Science and Technology of China in 1982 and 1984, respectively. From 1989 to 1993, she was an assistant professor in the Electrical and Computer Engineering Department, Wayne State University. She joined Ford Research Laboratory in 1993, where she worked in the Powertrain Control Systems Department. After spending almost 10 years in industry, she came back to academia and joined the faculty of the College of Engineering at the University of Michigan in 2003, where she is now a professor in the Department of Naval Architecture and Marine Engineering and the Department of Electrical Engineering and Computer Science. Her research interests include system and control theory and its applications to marine and automotive propulsion systems. She holds over 30 US patents and has co-authored a textbook on Robust Adaptive Control. She is an IEEE Fellow and one of the three recipients of the 2003 IEEE Control System Technology Award.

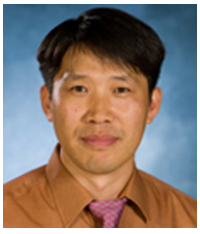

Soryeok Oh received his B.S. and M.S. degrees from Pusan National University, Pusan, South Korea in 1997 and 1999 and his Ph.D. degree from the University of Delaware, Newark, USA, in 2006, all in mechanical engineering. He is currently an assistant research scientist with the Naval Architecture and Marine Engineering Department at the University of Michigan, Ann Arbor, USA. He has a continuing interest in the area of power system dynamics control and modeling control of mechanical systems such as fuel cell/gas turbine hybrid systems, cable-suspended robots, marine vehicles, and UAVs.